Eur. Phys. J. B **37**, 127–136 (2004)
DOI: 10.1140/epjb/e2004-00037-9

THE EUROPEAN PHYSICAL JOURNAL B

Dissipation in the dynamics of a moving contact line: effect of the substrate disorder

S. Moulinet, C. Guthmann, and E. Rolley[a]

Laboratoire de Physique Statistique de l'École Nomale Supérieure, associé au CNRS et aux Universités Paris 6 et Paris 7, 24 rue Lhomond, 75231 Paris Cedex 05, France

Received 13 June 2003 / Received in final form 6 October 2003
Published online 19 February 2004 –

Abstract. We have studied the dynamics of the contact line of a viscous liquid on a solid substrate with macroscopic random defects. We have first characterized the friction force f_0 at microscopic scale for a substrate without defects; f_0 is found to be a strongly nonlinear function of the velocity U of the contact line. In presence of macroscopic defects, we find that the applied force $F(U)$ is simply shifted with respect to $f_0(U)$ by a *constant*: we do not observe any critical behavior at the depinning transition. The only observable effect of the substrate disorder is to increase the hysteresis. We have also performed realistic numerical simulation of the motion of the contact line. Using the same values of the parameters as in the experiment, we find that the experimental data is qualitatively well reproduced. In light of experimental and numerical results, we discuss the possibility of measuring a true critical behavior.

PACS. 46.65.+g Random phenomena and media – 64.60.Ht Dynamic critical phenomena – 68.08.Bc Wetting

1 Introduction

On many solid surfaces, the value of the contact angle depends on the way drops are deposited on the substrate. For a drop obtained by advancing the liquid-vapor interface, the value θ_a is larger than the value θ_r obtained after receding. This behavior is due to the pinning of the contact line (CL) on heterogeneities, which can be either due to chemical contamination or roughness. The presence of a local contamination change the local value $\theta(x, y)$ of the contact angle which depends on the position (x, y) on the substrate. In other words, the spreading coefficient $S \equiv \gamma(\cos\theta - 1)$ is a function of the position on the substrate (γ is the liquid-vapor surface tension). To some extend, a weakly rough substrate can also be described by a local spreading coefficient [1], but even a moderate roughness can lead to more complex situations [2].

Most recent theoretical works dealing with the properties of the contact line on a disordered substrate assume that the physics of the contact line (CL) is captured by a simple equation of motion similar to other equation proposed in the context of CDW or magnetic domain walls. Let Ox be the mean direction of the contact line and let $h(x, t)$ be the conformation of the CL, the equation of motion for the CL reads [3,4]:

$$\mu^{-1}\frac{\partial h(x,t)}{\partial t} = F + R(x, h(x,t)) - \frac{1}{\pi}\gamma\sin^2\theta_0 \int dx' \frac{h(x',t) - \overline{h(t)}}{(x-x')^2}. \quad (1)$$

The LHS is the friction force (μ is a dissipative coefficient that we shall call mobility), and the 3 terms in the RHS are respectively the external applied force F, the random force $R(x, y) = S(x, y) - \langle S\rangle$ due to the disorder of the substrate, and the elastic (capillary) restoring force [5]. All forces are per unit length.

Qualitatively, this model captures the main features of the dynamics of the CL, which is indeed similar to the one of other elastic systems in random media. When submitted to an increasing external force F, some part of the CL may jump, but the CL as a whole remains pinned until F exceeds a critical threshold F_C above which the mean velocity U is non zero. In other words, the CL does not advance until $\theta > \theta_a$, and $F_C = \gamma(\cos\theta_0 - \cos\theta_a)$, where θ_0 is the contact angle at equilibrium. Above the threshold, the CL advances through slow drifts and fast avalanches which have often been observed [6–8].

Above the threshold, one expects the mean velocity U of the CL to scale like $(F - F_C)^\beta$ where β is often called the velocity exponent. Ertas and Kardar have studied equation (1) using functional renormalization group (FRG)

[a] e-mail: rolley@physique.ens.fr

technique [4]. To first order in perturbation, they find $\beta \simeq 7/9$. Extending this calculation to two-loop order leads to $\beta \simeq 0.59$ [9]. There are also some discrepancies between numerical simulations. A direct numerical simulation leads to $\beta \simeq 1$ [10], while simulations using ad-hoc dynamical rules yield $\beta = 0.68 \pm 0.06$ [11].

A large number of experiments have been devoted to the measurement of $U(F)$ in a partial wetting situation, using various techniques: dipping filaments [12] or plates [13], capillary rise [7,14], ac method using the pressure response of liquid/liquid interface in capillaries [15] (additional references can be found in Ref. [7]). There is a large scatter in the fitted values of the exponent β ranging between 1 and 5. This is clearly inconsistent with the prediction of FRG calculation. However, the substrate is not characterized in these experiments. In most cases, the authors argue that the disorder is due to the roughness of the substrate, which can be changed to some extend by changing the sample [7] or etching the surface [15]. It is not obvious that the roughness has a short range correlation, a necessary condition for the model to apply. Furthermore, it is not obvious that the correlation length is macroscopic. If the pinning occurs at a microscopic scale, it is likely that the depinning transition is blurred because of thermal noise.

In this article we report an experiment designed to study the dynamics of the CL on a substrate with macroscopic defects and well characterized disorder. As a first step, and in order to completely characterize our system, we have measured the dissipation at microscopic scale on a substrate without macroscopic defects. We have found that the friction force $f_0(v)$ is not linear in the local instantaneous velocity v, contrary to what is assumed in equation (1), in which $f_0 = \mu^{-1}v$. Then, we have measured the force $F(U)$ which is needed for the system to advance with a mean velocity U on a random substrate. We find that $\delta F \equiv (F - f_0)$ is roughly independent on the velocity over three decades in U. In order to avoid any confusion, the notation f_0 will be used for the friction force at microscopic scale while F stands for the external force applied on the CL. Similarly, v is the local velocity while U is the mean velocity for the CL moving on a heterogeneous substrate.

We have performed a numerical simulation of equation (1), using the measured values of the friction force and the contact angles. We find again that, within the experimental range of velocity, δF is roughly constant, so that the shape of $F(U)$ is mainly controlled by the dissipation at microscopic scale. Measuring a true critical behavior turns out to be a challenging experiment.

We show also that the roughness of the CL, at the threshold, is not sensitive to the microscopic dissipation: the nonlinearity of f_0 cannot explain the anomalous value of the roughness exponent that we have measured in a previous experiment.

2 Experimental setup

2.1 Substrate and liquids

The substrate used here is similar to the one described in a previous experiment, where we studied the roughness and avalanche-like motion of the CL [8]. This substrate [P1] is a large glass plate partly covered with defects which consist of square patches of chromium (size 10×10 μm^2); the defects cover about 23% of the total area. The liquid is either pure water or a mixture of water and glycerol.

We have mainly studied the receding case. For water, and for $v \sim 1$ μm/s, the receding contact angle on glass without defect is $\theta_g \simeq 30°$ while on chromium $\theta_c = 40 - 50°$. For details on the cleaning procedure, we refer to [8].

This plate [P1] is rather thick and large, as it was designed for optical measurement of the CL roughness. In order to obtain an accurate measurement of the force, we have used a tensiometric technique, which requires the use of a thinner plate. The original pattern of [P1] was copied through a standard photolithographic process to both sides of a thin plate [P2] (thickness 0.15 mm). Through the process, the shape of individual defects has been slightly rounded, but the whole pattern is not significantly altered. The pattern covers only the bottom part [P2def] of the plate [P2]; the upper part [P2g] is bare glass. One can measure the change of the applied force when the meniscus sweeps the plate. θ_g is the same for [P1] and [P2g].

Measurements of $f_0(v)$ have been performed on a homogeneous plate [P3], which is in principle identical to [P2g] prior to the deposition of the pattern. Actually, both glasses are presumably not the same since we have observed that [P3] is slightly more wettable than [P2g]: $\theta_g \simeq 20°$. Yet, their properties are qualitatively similar, as shown in Section 3.

2.2 Optical measurements and force measurement

The spatial distortions of the receding CL have been studied optically. The results are reported in an earlier paper [8]. In the experiments reported here, the optical setup was used to monitor the pinning of the CL on a single defect. We have used a fast camera (215 frames/s) providing 8-bit images. The CL is defined as the position where the gray-level gradient is the steepest; the final resolution is 0.5 μm. Details about the setup and image analysis are given in reference [8].

The velocity vs. force relation $U(F)$ is measured by means of a home-build tensiometer shown in Figure 1. The plate to be studied is glued to the tip of a cantilever whose deformation is monitored by a capacitive sensor [16]. After calibration, the output voltage of the gauge can be converted to force. For the spring used here, we obtain a sensitivity of the order of 2 V/mN, and a resolution limited by the noise (a few mV). The main source of noise is the irregularities of the plate edges.

Provided that the dissipation occurs in the close vicinity of the CL, the measured force F_m is the sum of capillary forces and buoyancy force: $F_m = \gamma p \cos\theta + \rho g v_h$,

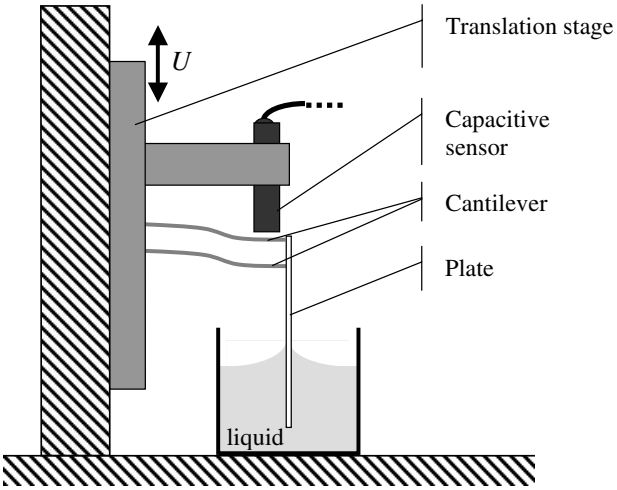

Fig. 1. Sketch of the experimental setup. The force acting on the plate induces a displacement of the cantilever which is monitored by a capacitive sensor; the velocity U is imposed by the translation stage.

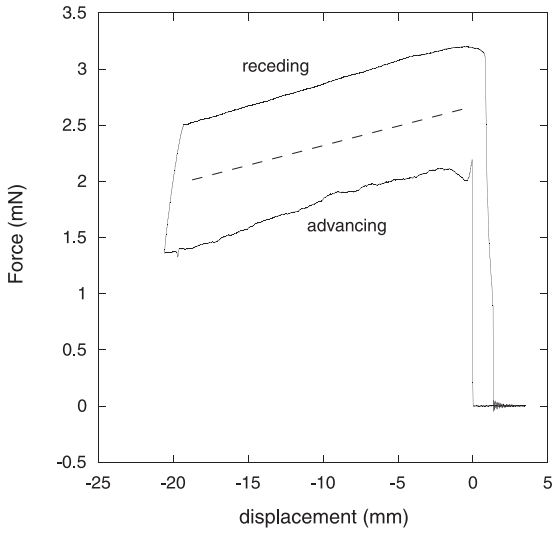

Fig. 2. Force as a function of the position of the translation stage during a cycle. The plate is dipped in water and withdrawn at a constant velocity $U_0 = \pm 100$ μm/s. The dashed line has the same slope as the contribution of the buoyancy force.

where $p = 48.3$ mm is the plate perimeter, ρ the density of the liquid g the acceleration of gravity and v_h is the volume of the plate below the liquid level.

The velocity is imposed by the translation stage, and can be varied between 1 and 1500 μm/s. The total displacement of the stage is typically 30 mm.The force F_m and the position x of the stage are recorded every 100 ms. Note that the displacement of the stage is not exactly the same as that of the plate, since the deformation of the spring changes with time. This effect is small since the maximum deformation of the spring with respect to the gauge is of the order of 300 μm.

A typical advancing-receding cycle at constant velocity is shown in Figure 2. The slope of the two branches is mainly due to the buoyancy force, but is generally slightly different. This means that θ is not exactly constant: there can be a shift of the order of a few degrees for a sweep of 30 mm. Moreover, there are also some small variations of θ from one run to the other. The scatter in the measurements of $\cos\theta$ is of the order of 0.03.

3 Dynamics at microscopic scale

Before addressing the question of the dynamics $U(F)$ of the CL on a substrate with macroscopic defects, it is necessary to wonder what are the actual dynamics $v(f_0)$ at a microscopic level.

In the simple model for the equation of motion (Eq. (1)), it is assumed that the friction force f_0 is linear in the velocity. Such an assumption is valid if the dissipation is due to shear flow in the meniscus. In this case, the dynamic contact angle is given by the Cox-Voinov relation [18]:

$$\theta_0^3 - \theta^3(v) = 9l\frac{\eta v}{\gamma} \tag{2}$$

where η is the viscosity and $l \equiv \ln(L/a)$ a logarithmic factor. L is a macroscopic cutoff length (the size of the drop or the capillary length) and a a microscopic cutoff; typical values of l fall in the range $5 < l < 15$ [17]. Note that, in equation (2), we have chosen U to be positive for a receding meniscus, because this is the experimental situation which we have studied. As we use f_0 instead of θ as a dynamic variable, equation (2) reads, for $\theta \simeq \theta_0$:

$$\frac{v}{f_0} = \mu = \frac{\theta_0^2}{3\eta l \sin\theta_0}. \tag{3}$$

Strictly speaking, θ_0 is the equilibrium contact angle. However, all real substrate show some hysteresis, and defining or measuring an equilibrium value is not simple. In order to take this hysteresis into account, it has been propose to use the value of the contact angle at zero velocity for θ_0. In some case, this leads to a reasonable agreement with experimental data [17]. For polar liquid such as water or glycerol, there is a clear disagreement, especially at low capillary number Ca ($Ca \equiv \eta v/\gamma < 0.01$) [17,20]. To explain this behavior, it has been proposed that the velocity of the CL could be limited by some other dissipation mechanism at the CL, such as molecular adsorption-desorption process on the substrate [19].

In order to completely characterize our experimental system, it was thus necessary to measure the actual $v(f_0)$ relation. A direct measurement was performed with the tensiometer. In a second step, we have analyzed the motion of the receding contact line when it meets an isolated defect.

3.1 Direct measurement of the friction force

We have measured $v(f_0)$ for the receding case for two reasons. The scaling behavior of the roughness of the CL has

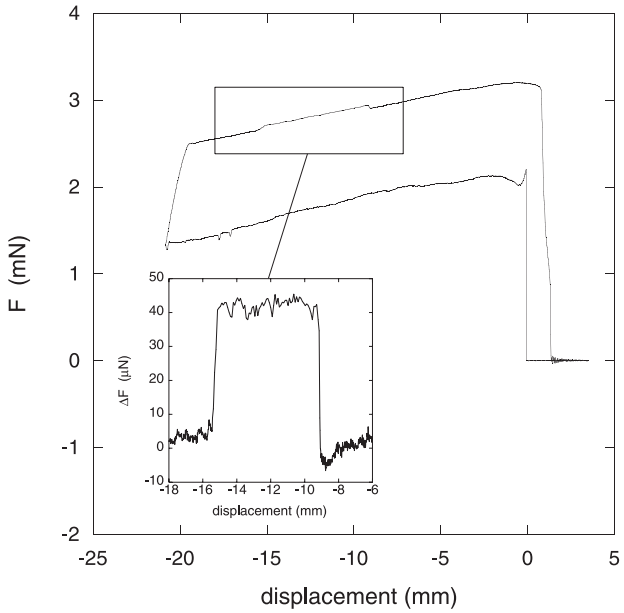

Fig. 3. Advancing-receding cycle. The plate is dipped in water and withdrawn at the velocity $v_0 = \pm 100$ μm/s, except for a short period where the velocity is increased to $v = 500$ $\mu m/s$. Inset: $F(v) - F(v_0)$ as a function of the position.

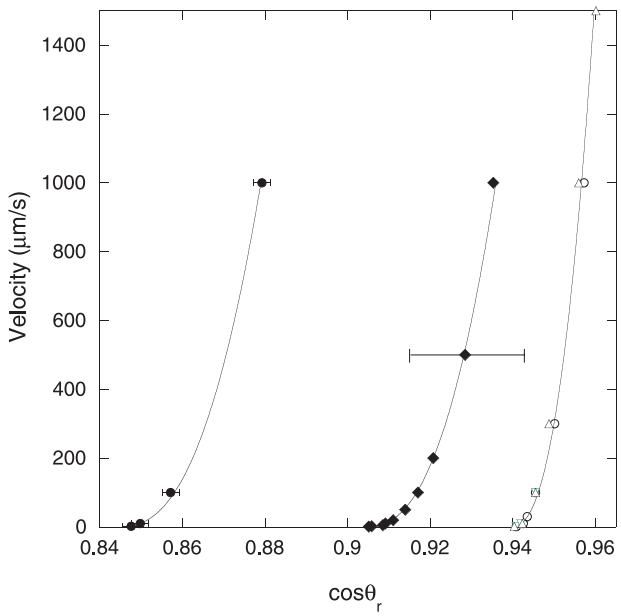

Fig. 4. Velocity v of the contact line as a function of $\cos\theta_r$. Black circles: [P2g]; diamonds: [P3] with low humidity level; open symbols: [P3] with high humidity level. The last data includes 3 different runs. Solid lines: fits with a power law $v = v_0(\cos\theta_r - \cos\theta_{ref})^{2.5}$.

been measured for a receding line. Also the value of the receding contact angle is more reproducible and less sensitive to the humidity level.

We have used the tensiometric technique described in Section 2.2. In order to suppress the scatter due to the slow drift and weak large scale heterogeneities of the substrate, we have used the following procedure. A reference cycle is done at constant velocity ($v_0 = 100$ μm/s). Then a second one is done at the same velocity, except on some parts of the cycle where another velocity U is imposed (Fig. 3). Subtracting the two curves yields a signal proportional to $F_m(v) - F_m(v_0) = p(f_0(v) - f_0(v_0))$ (see the inset of Fig. 3). If this is done repeatedly on the same part of the same plate, one obtains very reproducible differential measurements, even at low velocity.

Results for the plates [P2g] and [P3] are summarized in Figure 4, where the velocity is plotted as a function of $\cos\theta_r$.

For a given set of data, the relative uncertainty is small, of the order of the size of the symbols. It is larger for [P2g] because the photolithographic process has left some chromium patches outside the area where the pattern was copied. These few patches pin the CL and lead to some additional noise in the cycles. The relative position of the three data sets is known with a poorer accuracy, because absolute measurements of $\cos\theta$ are needed in this case. The corresponding uncertainty (of the order of ± 0.015 in $\cos\theta$) is shown by the large horizontal bar.

The results are sensitive to the humidity level, as shown by the two data sets for [P3]. With a water reservoir, and after a waiting time of two hours, we find smaller contact angles and a slightly steeper variation of v. When performed under the same conditions, the results are fairly reproducible.

It is obvious in Figure 4 that the velocity is a nonlinear function of $\cos\theta_r$. We have fitted the data by a power law $v = v_0(\cos\theta_r - \cos\theta_{ref})^{\alpha}$ with 3 adjustable parameters: v_0, θ_{ref} and α, using the same exponent α for the 3 data sets, one finds that a good agreement is obtained for a value of the exponent α between 2 and 3. It is interesting to compare our measurements with the prediction of equation (3). The slope of the 3 data sets is at most of the order of 10^5 μm/s for $v = 1000$ μm/s. Such a value leads to $l \sim 100$, which is unphysical. Thus viscous dissipation is certainly not relevant, at least in the range of capillary number $10^{-8} < Ca < 10^{-5}$.

3.2 Relaxation on a single defect

Some information on the dynamics of the CL can also be obtained by studying the relaxation of the contact line on a single defect. This has been done by Marsh and Cazabat [21] who measured the dynamics of the CL depinning from a single defect. After depinning, the CL shape is determined from equation (1) with $F = R = 0$. For a point-like defect and in the limit of small contact angles, one finds [22]:

$$h(x, t > 0) = \frac{-f_d}{2\pi\gamma\theta_0^2} \ln\left(\frac{x^2 + c^2t^2}{L^2}\right) \qquad (4)$$

where f_d is the defect force, $c = \mu\gamma\theta_0^2 = \gamma\theta_0^3/(3l\eta)$ and L an effective capillary length. Experimental data were found to be in good agreement with equation (4), though the fitted value of l was found to be anomalously low.

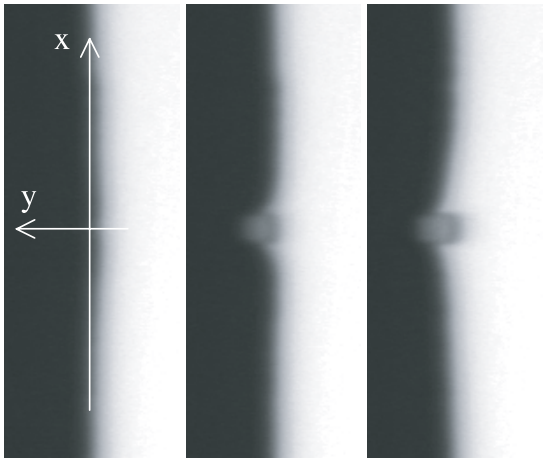

Fig. 5. Successive images of the CL uncovering a defect at times 0, 50, 350 ms. Actual width: 150 μm.

We have performed an experiment very similar to the one by Marsh and Cazabat. In our setup, the CL recedes on a glass plate at a constant mean velocity $U \sim 2$ μm/s. The plate is homogeneous, except for very few chromium defects. When the CL meets one of these, it jumps because chromium patches are less wettable than glass. Such an event is displayed in Figure 5. Let Ox be the direction of the CL, and let the origin O be the center of the defect side which is first met by the CL. The time origin is taken to be the meeting of the defect. The profile $h(x,t)$ of the CL is plotted as a function of t for various values of x, as shown in Figure 6. For each graph, we have plotted h for two values $\pm x$ symmetric with respect to the center of the defect. There are small differences between the opposite sides of the defect, which are presumably due to some weak large scale heterogeneities of the glass substrate. At large time, $\partial h/\partial t = U$. This asymptotic regime is reached earlier for large x, because the CL deformation is smaller.

In our system, f_0 is not proportional to v. Hence, we do not expect equation (1) to account for the measured $h(x,t)$. However, it is worth evaluating the magnitude of the disagreement. Let us assume $v = \mu f_0$. For a CL meeting a defect of negligible size in the x direction at $t = 0$, following [22], one finds:

$$h(x, t > 0) \sim -\ln\left(\frac{x^2 + c^2 t^2}{x^2}\right). \qquad (5)$$

This expression is valid only for $x \gg \xi$, and assumes that the defect exerts a constant force on the CL. However, we are interested in analyzing the whole shape. Also, as soon as the CL has completely uncovered the defect, the force on the CL is no longer constant; in this second step, the maximum deformation $h(0,t)$ is fixed. Thus, rather than using equation (5), we have performed a numerical integration of the equation of motion of the CL (Eq. (1)) which takes into account the features of the substrate: $R = 0$ everywhere, except for a square $\xi \times \xi$ defect where $R = \gamma(\cos\theta_c - 1)$. All coefficients are known, at least approximately, except μ.

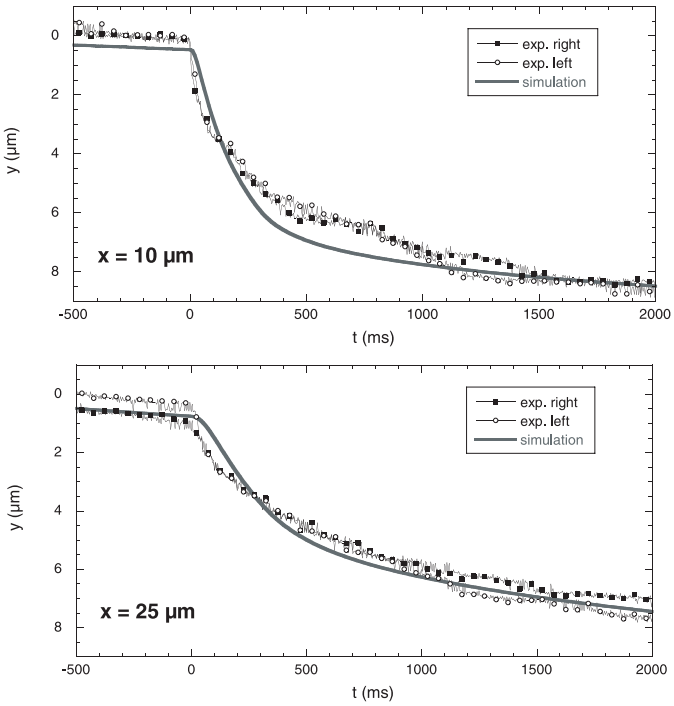

Fig. 6. Displacement y of the contact line as a function of t, for two positions $x = \pm 10$ μm and $x \pm 25$ μm. The solid line is the best fit for a friction force linear in velocity.

The solid lines in Figure 6 are the best fits obtained through this procedure, which leads to $\mu\gamma \sim 10^{-3}$ s/m. For $x = \pm 10$ μm, there is a clear disagreement with the experimental data: the measured velocity is much larger than the calculated one at early times. Let t_m be the instant at which the velocity is maximum. Within experimental accuracy, we always find that $t_m \simeq 0$, while the numerical solution leads to a value of t_m increasing with x similarly to the approximate solution of equation (5). For $x = \pm 25$ μm (lower Fig. 6), the disagreement is much less pronounced than for $x = \pm 10$ μm and the motion of the CL looks roughly consistent with the assumption $v = \mu f_0$. This is not surprising since the velocity dynamics is rather small as soon as $x > 3\xi$, which means that the actual $v(f_0)$ relation can be linearized. The fitted value of μ is consistent with the value of $(dv/df_0)_{v=U}$ obtained from the direct measurements discussed in Section 3.1. A more quantitative comparison is difficult because the two experiments have been performed on two different substrates.

The same experiment has been also performed with a mixture of water and glycerol whose viscosity was roughly hundred times larger than the viscosity of water. Quite surprisingly, we find the same curves $h(x,t)$ which are fitted by the same value of the mobility μ!

We have also tried to improve the poor fit in Figure 6 by using the measured $v(f_0)$ dependence. This leads to a steeper variation of h as a function of t at early times, in qualitative agreement with the observations. However, when the CL meets the defect, it experiences a very large local force, outside the range where $v(f_0)$ has been measured. In order to integrate the equation of motion, we

have to extrapolate $v(f_0)$, which leads presumably to a unrealistic high value of v. The fitting curves in Figure 6 rely not only on the hypothesis that $v(f_0)$ is linear, but also on the assumption that the deformation of the CL is small, so that the elastic restoring force is harmonic. In Figure 5, one can see that the deformation is strong in the vicinity of the defect. Thus, non harmonic corrections could also modify the shape of $h(x,t)$.

3.3 Discussion

In conclusion, the study of the relaxation on a single defects confirms the results reported in Section 3.1. The fitted value of the mobility μ is found to be roughly 10^3 smaller than expected from the simple hydrodynamic model for dissipation: equation (3) with $l = 10$ leads to $\mu\gamma \simeq 0.7$ s/m. Moreover, the fitted value of μ does not depend on the viscosity of the liquid. All together, these two experiments show that the dissipation at the contact line cannot be accounted for by simple hydrodynamics. The actual dissipation mechanism is certainly related to the microscopic structure of the contact line region (previous experiments at low capillary number have revealed a complex behavior [12,19]). It is likely that the heterogeneity of the glass surface is also responsible for the observed hysteresis.

In this paper, we are mostly interested in the dynamics of the CL on macroscopic defects. Due to the huge scale difference between the size of the defects (10 μm) and the microscopic scale of the glass heterogeneities, we assume that we can forget about the microscopic structure of the CL: we consider the measured friction force as a phenomenological ingredient in the equation of motion for the CL. In the following, we will assume that, for a homogeneous substrate and for velocities in the range $1 - 1000$ μm/s, $v = v_0(\cos\theta_r - \cos\theta_{ref})^\alpha$ with $\alpha \simeq 2.5$. Previous analysis of the CL dynamics during a fast jump on a defect has shown that the maximum instantaneous local velocity is of the order of 1 mm/s [8], so that the range in which we have measured the friction is large enough.

At this point, one should note that the force $f_0 = \gamma(\cos\theta_r - \cos\theta_0)$ is known only within a constant: the equilibrium contact angle θ_0 is unknown since there is some hysteresis even for an homogeneous glass plate. Exactly the same difficulty arises when one tries to compute $S = \gamma(\cos\theta_0 - 1)$. However, only the balance of capillary and friction forces is relevant in the equation of motion. Thus, we are allowed to use θ_{ref} (the fitted value at which the velocity vanishes) instead of the true equilibrium contact angle, as long as we are dealing only with a receding CL. Hereafter, by a slight abuse of notation, we shall use the following consistent definitions for S and f_0: $S = \gamma(\cos\theta_{ref} - 1)$ and $f_0 = \gamma(\cos\theta_r - \cos\theta_{ref})$. Of course, this is valid because we analyze the dynamics of a CL which is always receding: the contact angle is always smaller than θ_{ref} so that the sign of f_0 is constant. Stated another way, the CL cannot realize what is the equilibrium contact angle and how large is the hysteresis if it keeps moving always in the same direction.

4 Dynamics at macroscopic scale

We are now interested in the behavior of the CL on a substrate with many macroscopic defects. Let us first recall the usual simple picture of the depinning transition [4]. Assuming that the friction force at microscopic scale is linear in velocity ($v = \mu f_0$), the characteristics $U(F)$ is expected to have the shape sketched in Figure 7. Close to the threshold, $U \propto (F - F_C)^\beta$, with $\beta < 1$; at large force, the disorder is not relevant and one recovers $U \sim f_0$. In other word, the supplementary force due to the pinning $\Delta F = F - f_0$ is a decreasing function of U.

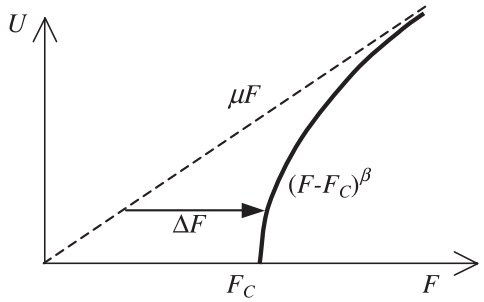

Fig. 7. Sketch of the expected $U(F)$ dependence for a disordered substrate.

We have seen in the previous section that the relation $v(f_0)$ cannot be obtained by a simple hydrodynamic argument. It has to be measured, and is dependent on the nature of the glass plate and on the humidity. Moreover, at a fixed velocity, some variation of f_0 can be measured along the plate. In order to avoid systematic uncertainties, we choose again to perform differential measurements. To this aim, we have designed a substrate on which the defects cover only the bottom part of the plate [P2]. Hysteresis cycles for two different velocities are shown in Figure 8. One clearly observes the jump in force when the CL crosses the boundary between the bare glass [P2g] and the glass covered with the chromium pattern [P2def]. In order to make the jump more visible, the mean tilt of the hysteresis cycle has been subtracted in the lower graph in Figure 8.

As seen in Figure 8, the jump is not very sharp, and the transition is completed after the plated has travelled by roughly 1.5 mm. There is certainly a finite transient between the two stationary states, but this is also due to the fact that the boundary of the chromium pattern is not very sharp and is not quite horizontal. Whatever the velocity, the jump has the same shape, which means that the transient must be very short. This is in agreement with direct observation of the CL configuration: after a sudden velocity change, a stationary state is reached as soon as the CL has moved by a few hundreds of micrometers.

It is obvious from Figure 8 that the jump in force is almost independent on the velocity. More precisely, one finds that the jump in force $\delta F/\gamma = -0.037 \pm 0.003$ for $1 \leq U \leq 300$ μm/s. For the highest velocity ($U = 1000$ μm/s), it seems that $|\delta F|$ is slightly larger, but the change is of the order of the uncertainty. At first sight, the negative sign of δF may look strange in view of Figure 7. One should

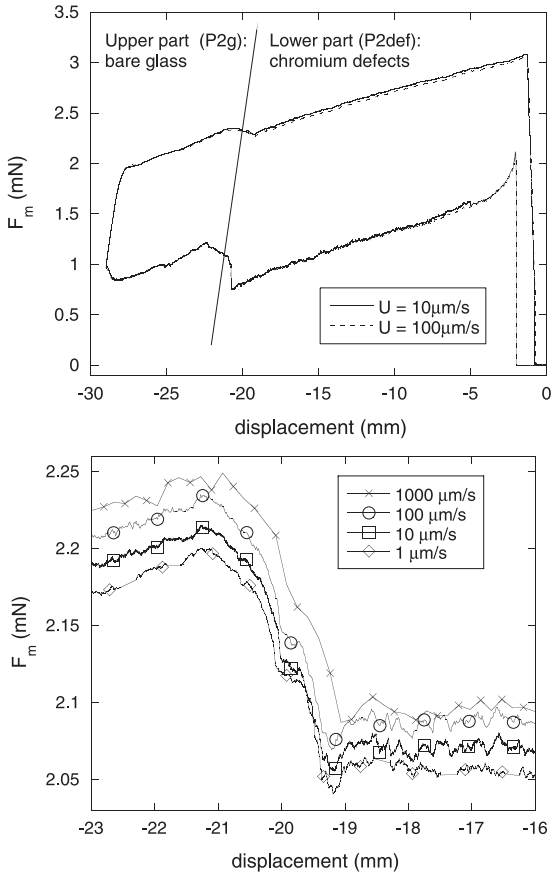

Fig. 8. Upper graph: hysteresis cycle for the plate [P2] half covered by the chromium pattern. Lower graph: jump of the measured force F_m at the boundary for the CL receding at various velocities. The mean tilt of the cycle has been subtracted and the curves have been shifted for clarity.

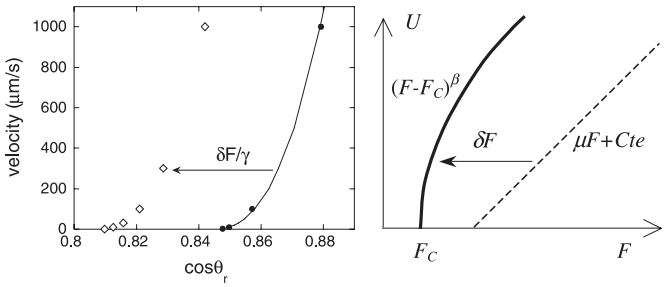

Fig. 9. Left: measured velocity-$\cos\theta_r$ dependence. Full circles: homogeneous glass substrate [P2g]; diamonds: substrate with defects [P2def]. Right: sketch of the expected theoretical velocity-force characteristics in the case where the homogeneous substrate (dashed curve) is, on average, more wettable than the disordered substrate (full curve).

realize that $\delta F > 0$ only if the mean spreading coefficient $\langle S\rangle$ (or mean contact angle) is the same for both the homogeneous and heterogeneous substrate. This is the usual assumption in theoretical works where it is easy to design a substrate with more wettable and less wettable defects in equal number. This is not the case in the experiment; to avoid confusions, the shift in force is written δF instead of ΔF when all defects are less wettable than the bare substrate. Thus, the shift δF is the result of two opposite effects: (i) the patterned substrate [P2def] is, *on average*, less wettable than glass, which leads to a negative contribution to δF. (ii) the patterned substrate is heterogeneous, which leads to a threshold in force and a positive contribution to δF. When considering the upper graph in Figure 8, it is clear that the presence of the defects do increase the hysteresis.

The actual situation is summarized in Figure 9. In the left graph, the measured velocities are plotted as a function of $\cos\theta_r$ instead of the applied force. We have first plotted the data for the homogeneous glass substrate [P2g]: $v = a(\cos\theta_r - \cos\theta_r ef)^\alpha$. For the disordered substrate [P2def], data are obtained by shifting the data for [P2g] by $\delta F/\gamma$. In the right graph of Figure 9, we have sketched the expected theoretical δF if the friction force (dashed curve) is measured on a homogeneous substrate whose wettability is larger than the average wettability of the disordered substrate, as it is the case for [P2g] and [P2def]. Theoretical models predict that $|\delta F/\gamma|$ increases with the velocity.

Within experimental accuracy, it is clear that the only consequence of the disorder is to shift the force necessary to make the line recede. There is no evidence of a critical behavior: the shape of the velocity-force characteristic is entirely dictated by the friction force at microscopic scale. However, one still has to check whether we have explored the right velocity range. For the highest velocity, of the order of 1 mm/s, the friction force is of the order of 0.03γ; the amplitude of the disorder is $\Delta S \equiv \sqrt{\langle (S - \langle S\rangle)^2\rangle}$. It is easily estimated from the values of the contact angles on glass and chromium; one finds $\Delta S \simeq 0.1\gamma$. Thus, the critical behavior, if any, should be observed in the experimental range of velocity.

Finally, let us also remark that δF is independent on the velocity also for the advancing contact line (upper Fig. 8).

5 Numerical simulation of the experiment

Our results cannot be compared with the (FRG) solution of the dynamical equation (1), because the friction force is not linear in our experiment. Thus, the left term in equation (1) ($f_0 = \mu^{-1}(\partial h/\partial t)$) should be changed to:

$$f_0 = \gamma \left(\frac{1}{v_0} \frac{\partial h(x,t)}{\partial t} \right)^{1/\alpha}. \qquad (6)$$

The parameters v_0 and α have to be determined from the experimental measurements of the friction force (Sect. 3.1). This leads to a nonlinear equation, whose general study is well beyond the scope of the present work. Our modest goal is to determine whether this equation can describe the measured dynamics of the CL. We have performed a numerical simulation of the contact line which is restricted to the values of the parameters which are used in the experiment.

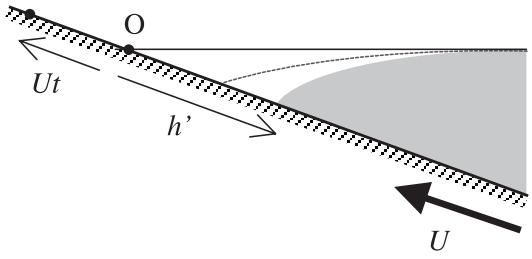

Fig. 10. The position $h' = h - Ut$ of the CL in the laboratory frame is measured from the intercept of the plate and the asymptotic liquid-vapor interface. The CL on a plate with chromium defects is shifted with respect to its position on a homogeneous glass substrate (dashed line).

5.1 Numerical integration of the equation of motion

In the simulation, as in the experiment, the plate is withdrawn from the liquid at a constant velocity U. The geometry is the same as in the optical study of the CL roughness [8]: the plate is tilted with respect to the horizon by an angle ϕ smaller than θ (Fig. 10). Let $h(x,t)$ be the position of the CL with respect to the moving substrate, and let $h'(x,t) = h(x,t) - Ut$ be the position of the CL in the laboratory frame. The local force balance can be written as:

$$f_0 = -S(x, h(x,t)) - \gamma(1 - \cos\overline{\theta}) + \mathcal{K}[h] \qquad (7)$$

where f_0 is now given by equation (6), $\mathcal{K}[h]$ is the elastic restoring force, and $\overline{\theta}$ is the average contact angle. The expression of $\mathcal{K}[h]$ (last term in the RHS of Eq. (1)) involves the factor $\sin^2\theta_0$; here, we used the actual value of the receding contact angle $\overline{\theta} \simeq \theta_{ref}$ instead of θ_0. $\overline{\theta}$ is related to the mean value $\overline{h'}$ of h' along the line by: $\overline{h'} = L'_C(1 - \cos(\overline{\theta} - \phi))^{1/2}$, where ϕ is the tilt of the substrate and $L'_C \equiv \sqrt{2\gamma/(\rho g)}/\sin\phi$. The force acting on the plate, which would be measured in an experiment, is simply $\gamma\cos\overline{\theta}$. In order to emphasize the possible effect of the non linearity in f_0, we choose the higher value of α compatible with the experiment ($\alpha = 3$).

In order to solve equation (7), we use exactly the same scheme as Zhou [10]. We first discretize space in the x direction using a uniform spacing Δx; we impose periodic boundary conditions along x. We then have a set of ordinary differential equations in $h(x_i,t)$ which we solve using the adaptive step-size second order Runge-Kutta method. The elastic restoring force is a convolution which is best calculated in the Fourier space using Fast Fourier Transforms [10]. The first term can be calculated in real space from the local spreading coefficient $S(x,y)$ which has the same properties as in the experiment. It can take two values corresponding to the contact angles θ_{ref} on glass and on chromium defects (respectively 30 and 55°). The positions of the defects are completely random, and the coverage is the same as in the experiment (0.23). The spacing Δx is equal to the defect size $\xi = 10$ μm, and the width of the sample is 1024. The equivalent width (10 mm) is of the order of the capillary length so that finite size effect should be similar in the simulation and in the experiment.

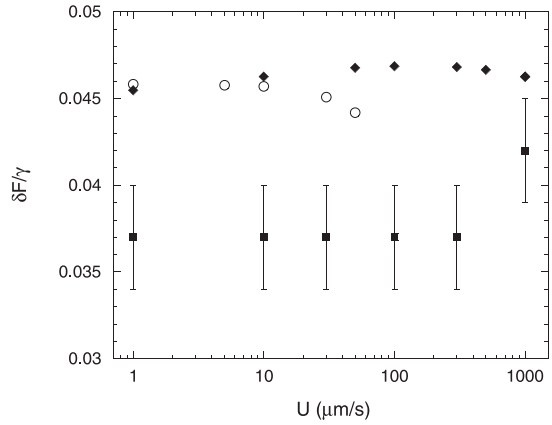

Fig. 11. Shift in force $\delta F/\gamma$ between a substrate with defects and a reference glass substrate. Black squares: experimental data; diamonds: simulation with nonlinear friction force ($f_0 \propto U^{-1/3}$); circles: simulation with a linear friction force ($f_0 \propto U$).

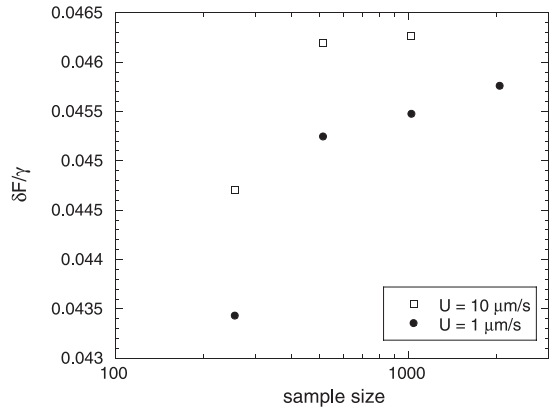

Fig. 12. $\delta F/\gamma$ as a function of the system size.

5.2 Results

The results of the simulation are shown in Figure 11. We have plotted the shift in force $\delta F/\gamma$ between a substrate with defects and a reference glass substrate. In the whole velocity range, we find that $|\delta F|$ is roughly constant, in agreement with the experimental results. Moreover, the numerical value $\delta F/\gamma = -0.046$ obtained from the simulation is close to the experimental one (-0.037). A good numerical agreement could be achieved by choosing 50° instead of 55° for the value of the contact angle on the chromium defects. The value $\theta_{Cr} = 50°$ would be consistent with the measured value of the receding contact angle on chromium (40 to 50°). The value $\theta_{Cr} = 55°$ is a compromise, chosen in order to obtain roughly the same amplitude of the CL fluctuations as in the experiment (see next section).

When looking carefully at the data from the simulation, a small decrease can be observed at low velocity, which could be considered as the beginning of a critical regime. However, as shown in Figure 12, the value of δF depends on the size of the sample. For velocities smaller than 10 μm/s, a sample width of 1024 is presumably not large enough. This is a usual difficulty in such depinning simulations, as the correlation length of CL fluctuations

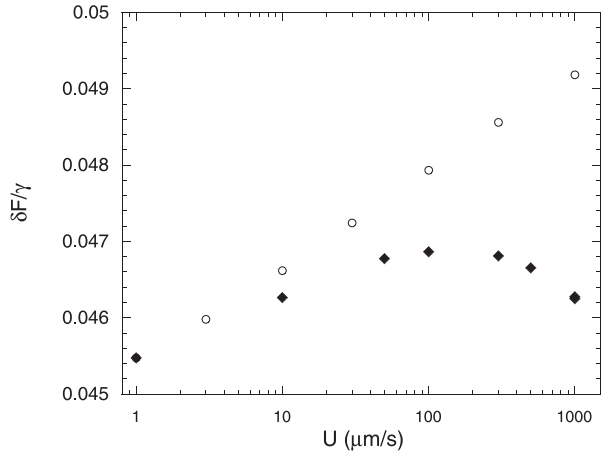

Fig. 13. Plot of $\delta F/\gamma$ as a function of the velocity; circles: the stiffness of the contact line is constant (usual assumption); diamonds: the stiffness decreases as $\sin^2\overline{\theta}$ (realistic simulation).

diverges at the threshold. One should realize that such a difficulty is also an experimental one: our experimental system is presumably slightly too small to determine accurately a critical behavior.

We have to stress here that equation (7) is slightly different from the equations of motion which have been previously studied, both numerically and analytically. In our simulation, which is intented to mimic the experiment, the elastic restoring force $\mathcal{K}[h]$ of the line is controlled by the factor $\sin^2\overline{\theta}$, where $\overline{\theta}$ is the actual mean contact angle and thus depends on the velocity. Qualitatively, this dependence has the following effect: when the velocity increases, the contact angle and the stiffness of the CL decrease, so that it becomes more pinned. As a consequence, the velocity increases more slowly with the applied force than it would increase if the stiffness were constant. In the experimental range, one finds that $\overline{\theta}$ decreases from 30 down to 26° when U increases from 1 to 10^3 μm/s. This is a small variation, but is leads to a decrease in the CL stiffness by 25 per cent, which is not negligible. In Figure 13, we have plotted $\delta F(U)$ when $\overline{\theta}$ and the CL stiffness are kept constant: an increase of $\delta F(U)$ can now be observed. Thus, one has to be vary careful when comparing the measured behavior with theoretical prediction, because the critical behavior can be masked or modified by the variation of the control parameter with the velocity. The worst case is the one of small angles, because of the quadratic dependence of the stiffness with $\overline{\theta}$. In principle, working at very low velocity decreases this effect. However, we stress that finite size effects can be important at low velocity.

To summarize, the results of the simulation are in agreement with the experiments: δF is almost independent on the CL velocity. The simulation tells us also that there could exist a very small critical variation, but (i) this variation is of the order of the accuracy of our setup and (ii) this variation may be not universal. One should be careful about finite size effect and about variation of CL stiffness.

6 Conclusion

Our main experimental results are: (i) the friction force f_0 measured on a smooth substrate is nonlinear in the velocity. The microscopic mechanism responsible for this behavior is not clear; it is presumably related to the existence of an absorbed film since the friction depends on the humidity level. (ii) When macroscopic defects are added, one observe the usual jerky motion of the CL due to pinning on the defects. The force F which has to be exerted on the plate is simply shifted by a *constant* δF. Note that the range for the mean velocity U is such that the dissipative force $f_0(U)$ is always smaller than the disorder strength ΔS, so that the system is close to the depinning threshold.

It is interesting to come back to earlier experiments. Our observations are very similar to the ones of Kumar et al. [15]. They have measured the ac response dF/dU of a liquid-liquid interface in capillaries as a function of the velocity U. They find that the hysteresis is larger for etched (rough) tubes than for standard (smooth) tubes. In both cases, they measure the same ac response, which leads to $U \propto (F - F_C)^\beta$ with $\beta \simeq 5$. Their conclusion is that they found a universal depinning behavior characterized by a velocity exponent $\beta \simeq 5$. Our interpretation is rather than this "universal" behavior has nothing to do with a depinning transition: dF/dU does not depend on the presence of macroscopic defects and it is entirely controlled by a microscopic dissipation mechanism which is not viscous. One may argue that this microscopic dissipation mechanism is nothing but pinning on microscopic or mesoscopic defects. In this case, one cannot neglect thermal noise, so that the nature of the depinning transition is modified. A direct evidence for thermal activation near the depinning threshold has been given by Prevost et al. [23] Moreover, in view of the large dispersion (1 to 5) in the fitted values of β obtained in various experiments, or even in various runs of the same experiment, there is a clear lack of "universality."

An interesting question is whether the non linearity in the friction force $f_0(v)$ has an impact on the CL behavior at the depinning threshold. We have performed the same simulation as described in Section 5.1 with $f_0 = \mu^{-1}v$, for velocities U such that $10^{-3} < U/(\mu\Delta S) < 10^{-1}$. As shown in Figure 11, we find again that δF is roughly independent of U. A decrease of δF can be observed for $U > 50$ μm; this is because the mobility ($\gamma\mu = 10^{-3}$ s/m)obtained from low velocity data (see Sect. 3.2) yields an overestimate of the dissipation at high velocity. Though $f_0 \propto v$, the data from the simulation do not allow us to determine the critical exponent β because, as stressed earlier, the stiffness of the CL is not kept constant in the simulation and because the data at low velocity depends on the sample size. At this point, we can only say that, in such an experiment as ours, one cannot measure the signature of a non linearity in f_0.

Finally, one may wonder if the non linearity of $v(f_0)$ has an impact on the scaling behavior of the roughness W at the depinning threshold. We define W as: $W(L) = \left\langle\left\langle(\eta(L+x) - \eta(x))^2\right\rangle\right\rangle^{1/2}$ (the average is taken

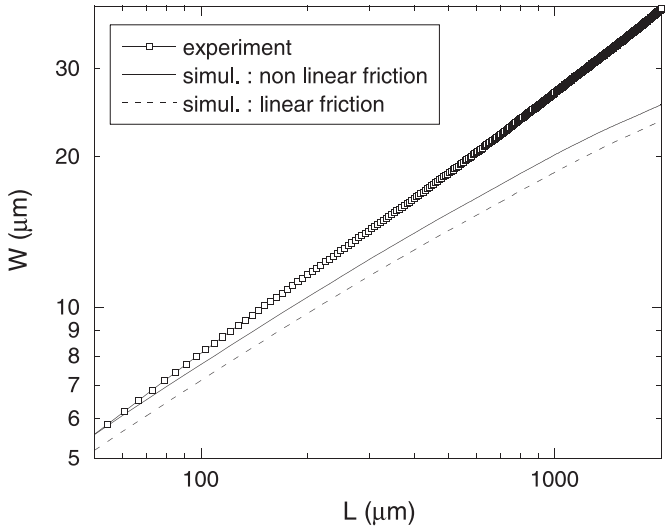

Fig. 14. Scaling behavior of the roughness W of the CL for both experiment (liquid: water; $U = 20$ μm/s [8]) and simulations. The result of simulations is independent of the nature of the friction: $W(L)$ is the same for $v \propto f_0$ and for $v \propto f_0^3$ (the small shift is due to a small difference in θ_{ref} between the two cases).

over x along the line and over successive configurations of the CL). One expects W to vary with the scale L as L^{ζ}, where ζ is called the roughness exponent. Results of the simulation for $W(L)$ are shown in Figure 14 for both cases: $v \propto f_0$ and $v \propto f_0^3$, with numerical coefficients taken from the experiment. The two curves are identical: the non linearity in the friction force does not change the scaling of the CL roughness. Fitting the curves in the range $10\xi < L < 1$ mm leads to $\zeta \simeq 0.40$, in reasonable agreement with the prediction by Rosso and Krauth [24]. In Figure 14, we have also plotted the measured roughness $W(L)$ obtained in a previous experiment [8]. It can be seen that the measured value of the roughness exponent ($\zeta = 0.51 \pm 0.03$ [25]) cannot be explained by the non linearity in $v(f_0)$. The order of magnitude for W is consistent with the result of the simulation, but we have chosen the disorder strength (that is the value of θ_{Cr}) for that purpose. One should notice rather that we cannot obtain an agreement for both δF and W with a single value of the disorder strength.

It turns out that the measured properties of the CL close to the depinning threshold, $W(L)$ and $\delta F(U)$, are not sensitive or only weakly sensitive to the non linearity in $v(f_0)$, at least in the parameter range that we have explored. This is not so surprising, since we have seen in Section 3.2 that the motion of the CL was approximately fitted when linearizing the $v(f_0)$ relation.

In conclusion, both experiment and simulation show consistently that the shape of the $U - F$ characteristics is mainly dictated by the dissipation at microscopic scale. Thus, this dissipation has to be properly characterized and $U(F)$ has to be accurately measured in order to be able to distinguish a possible critical behavior. There is not such difficulty in determining the roughness exponent; however, its measured value is in disagreement with theoretical predictions. Most of the physical ingredients in the equation of motion are under control: we have checked previously that the motion is quasistatic, the disorder is well characterized, the friction has been measured... What could be wrong? Maybe a non harmonic correction to the elastic energy could lead to a change in the roughness exponent, as shown by Rosso and Krauth in the case of local elasticity [26].

We thank X. Noblin for designing the tensiometer; W. Krauth, A. Rosso and P. Le Doussal for helpful discussions.

References

1. P.G. de Gennes, Rev. Mod. Phys. **57**, 827 (1985)
2. S.M.M. Ramos, E. Charlaix, A. Benyagoub, M. Toulemonde, Phys. Rev. E **67**, 031604 (2003)
3. M.O. Robbins, J.F. Joanny, Europhys. Lett. **3**, 729 (1987)
4. D. Ertaç, M. Kardar, Phys. Rev. E **49**, 2532R (1996)
5. J.F. Joanny, P.G. de Gennes, J. Chem. Phys. **81**, 552 (1984)
6. E.L. Decker, S. Garoff, Langmuir **13**, 6321 (1997)
7. E. Schäffer, P.Z. Wong, Phys. Rev. E **61**, 5257 (2000)
8. S. Moulinet, C. Guthmann, E. Rolley, Eur. Phys. J. E **8**, 437 (2002)
9. P. Chauve, P. Le Doussal, K.J. Wiese, Phys. Rev. Lett. **86**, 1785 (2001)
10. Y. Zhou, *Critical dynamics of contact lines,* Ph.D. thesis, John Hopkins University, Baltimore 1999
11. S. Ramanathan, D. Fisher, Phys. Rev. B **58**, 6026 (1998)
12. A. Schwartz, S.B. Tejeda, J. Colloid Interface Sci. **38**, 359 (1972)
13. G. Ström, M. Frederiksson, P. Stenius, B. Radoev, J. Colloid Interface Sci. **134**, 107 (1990)
14. T.E. Mumley, C.J. Radke, M.C. Williams, J. Colloid Interface Sci. **109**, 398 (1986)
15. S. Kumar, D.H. Reich, M.O. Robbins, Phys. Rev. E **52**, 5776R (1995)
16. Capacitive displacement sensor Micro-Epsilon, model capaNCDT 610, equipped with sensor S601-0,5
17. S. Kistler, in *Wettability*, edited by J.C. Berg (Marcel Dekker, New York, 1993)
18. R.G. Cox, J. Fluid Mech. **168**, 169 (1986)
19. T.D. Blake, in *Wettability*, edited by J.C. Berg (Marcel Dekker, New York, 1993)
20. R.A. Hayes, J. Ralston, J. Colloid Int. Sc. **159**, 429 (1993)
21. J.A. Marsh, A.M. Cazabat, Phys. Rev. Lett. **71**, 2433 (1993)
22. P.G. de Gennes, C.R. Acad. Csi, Ser II **302**, 731 (1993)
23. A. Prevost, E. Rolley, C. Guthmann, Phys. Rev. Lett. **83**, 348 (1999)
24. A. Rosso, W. Krauth, Phys. Rev. E **65**, 025101(R) (2002)
25. This value has been obtained by analysing the scaling of $W(L)$ [8]. A more recent analysis of the distribution of line width confirms the value $\zeta \simeq 0.50$ (S. Moulinet, A. Rosso, W. Krauth, E. Rolley, `cond-mat/0310173`, submitted to Phys. Rev. E)
26. A. Rosso, W. Krauth, Phys. Rev. Lett. **97**, 187002 (2001)